INTERNATIONAL JOURNAL FOR NUMERICAL METHODS IN FLUIDS, VOL. 11, 453–477 (1990)

# TWO-DIMENSIONAL SLOSHING ANALYSIS BY LAGRANGIAN FINITE ELEMENT METHOD

TAKASHI OKAMOTO

*Steel Research Center, NKK Corporation, Kanagawa, Japan*

AND

MUTSUTO KAWAHARA

*Department of Civil Engineering, Chuo University, Kasaga 1-chome 13, Bunkyo-ku, Tokyo, Japan*

## SUMMARY

Two dimensional sloshing analysis has been carried out by the Lagrangian finite element method. For the integration in time, the velocity correction method with the same interpolation functions for velocity and pressure is successfully used. The Lagrangian treatment to pursue the free surface position is presented. The comparison with the experiments shows extremely good agreement. It is shown that the large amplitude sloshing waves in a container can be analyzed by the present method.

KEY WORDS Finite element method Lagrangian description Velocity correction method Sloshing analysis Waves in a container

## 1. INTRODUCTION

Sloshing is the liquid motion of a free surface in a container subjected to forced oscillation. In engineering problems, analyses of sloshing are very important, e.g. liquid oscillations of large storage tanks caused by earthquakes, liquid motions of containers of tankers caused by swaying and rolling motions during sailing, and motions of liquid fuel in tanks of aircraft and spacecraft.

A number of studies have been presented on sloshing analyses, but most of them are based on linear theory[1–4], i.e. sloshing wave heights are assumed to be small and a linearized free surface boundary condition is assumed. When the amplitude of the forced oscillation is small, linear theory is valuable and has proved successful in the design of tanks and containers. When the amplitude of the forced oscillation is large or the excitation of the forced oscillation is near the natural frequency of the liquid, a large sloshing wave occurs. Various studies[5–23] have been presented on sloshing motions of finite amplitude, but the shapes of the containers have been limited to simple ones, i.e. rectangular or circular and without roofs or chamfers.

This paper presents the two-dimensional analysis of large-amplitude sloshing waves in containers which have roofs or chamfers by the Lagrangian finite element method. Using the Lagrangian description, the liquid always agrees with the region to be analysed. This is of great advantage in solving the free surface problem and one can easily treat complex shapes of containers.

For the analytical procedure the velocity correction method has been applied. This method has been investigated by many authors, including Ramaswamy *et al.*,[12] Ramaswamy and Kawahara,[13,14] Kawahara and Anjyu[15] and Okamato *et al.*[16] In this paper a treatment of the free surface flow on a multi-sloped wall boundary is advanced.

0271–2091/90/130453–25$12.50

*Received April 1989*
*Revised October 1989*

The numerical results computed are compared with the experimental results in order to investigate the validity of the present method. Another two sloshing analyses are presented of liquids in complex containers with roofs or chamfers.

## 2. BASIC EQUATIONS

The equation of motion and the equation of continuity in Lagrangian form are given by

$$DU_i/Dt = -p_{,i}/\rho + \upsilon(U_{i,j} + U_{j,i})_{,j} + f_i, \tag{1}$$

$$U_{i,i} = 0, \tag{2}$$

where $U_i$ and $f_i$ are the velocity and acceleration respectively in the $x_i$-direction ($i = 1, 2$), $p$ is the pressure, $\rho$ is the density and $\upsilon$ is the coefficient of kinematic viscosity. $DU_i/Dt$ represents the material derivative of the velocity.

The following two kinds of boundary conditions are used in this analysis. One is assumed to be the boundary on the rigid wall (on $S_1$) and the other is the boundary on the free surface (on $S_2$):

$$U_i = \hat{U}_i, \quad Q = p_{,i}n_i = \hat{Q} \quad \text{on } S_1, \tag{3}$$

$$p = \hat{p}, \quad T_i = \upsilon(U_{i,j} + U_{j,i})n_j = \hat{T}_i \quad \text{on } S_2, \tag{4}$$

where $\hat{U}_i$, $\hat{Q}$, $\hat{p}$ and $\hat{T}_i$ are given values on the boundaries and equation (4) is an approximate free surface boundary condition.

## 3. VELOCITY CORRECTION METHOD

In the Lagrangian description the material acceleration is approximated as follows:

$$DU_i/Dt \simeq (U_i^{n+1} - U_i^n)/\Delta t, \tag{5}$$

$$U_i^n = U_i(t_n, x_i^n), \tag{6}$$

$$U_i^{n+1} = U_i(t_n + \Delta t, x_i^{n+1}), \tag{7}$$

$$x_i^{n+1} = x_i^n + \Delta t(U_i^{n+1} + U_i^n)/2, \tag{8}$$

where $\Delta t$ is the time increment, $x_i^n$ and $x_i^{n+1}$ are the positions of the fluid particle at times $t^n$ and $t^n + \Delta t$ respectively and $U_i^n$ and $U_i^{n+1}$ are the particle velocities at steps $n$ and $n+1$ respectively.

The velocity correction method based on the Lagrangian formulation[13] is applied in this paper. The following calculation procedure can be derived.

1. Calculate the intermediate velocity $\tilde{U}_i^{n+1}$ by

$$\tilde{U}_i^{n+1} = U_i^n + \Delta t[\upsilon(U_{i,j}^n + U_{j,i}^n)_{,j} + f_i^n]. \tag{9}$$

2. Solve the Poisson equation for $p^{n+1}$ by

$$p_{,ii}^{n+1} = (1/\Delta t)\tilde{U}_{i,i}^{n+1}. \tag{10}$$

3. Correct $\tilde{U}_i^{n+1}$ by

$$U_i^{n+1} = \tilde{U}_i^{n+1} - \Delta t p_{,i}^{n+1}. \tag{11}$$

Steps 1–3 are repeated until the preassigned total time is reached.

## 4. FINITE ELEMENT FORMULATION

The equations of motion and continuity are multiplied by the weighting functions $U_i^*$ and $p^*$ respectively and integrated over the domain $V$. Integrating by parts in equations (9) and (10) and using the divergence theorem, the weighted residual equations corresponding to equations (9)–(11) are derived as follows:

$$\int_V (U_i^* \tilde{U}_i^{n+1})\mathrm{d}V = \int_V (U_i^* U_i^n)\mathrm{d}V + \Delta t\left(-\upsilon \int_V [U_{i,j}^*(U_{i,j}^n + U_{j,i}^n)]\,\mathrm{d}V + \int_V (U_i^* f_i^n)\mathrm{d}V + \int_S \{U_i^*[\upsilon(U_{i,j}^n + U_{j,i}^n)]n_j\}\,\mathrm{d}S\right), \tag{12}$$

$$\int_V (p_{,i}^* p_{,i}^{n+1})\mathrm{d}V = -(1/\Delta t)\int_V (p^* \tilde{U}_{i,i}^{n+1})\mathrm{d}V + \int_S (p^* p_{,i}^{n+1})n_i \mathrm{d}S, \tag{13}$$

$$\int_V (U_i^* U_i^{n+1})\mathrm{d}V = \int_V (U_i^* \tilde{U}_i^{n+1})\mathrm{d}V - \Delta t \int_V (U_{,i}^* p_{,i}^{n+1})\mathrm{d}V. \tag{14}$$

The natural boundary conditions of equations (12) and (13) correspond to equations (4) and (3) respectively.

Velocity $U_i$, pressure $p$ and the corresponding weighting functions $U_i^*$ and $p^*$ are interpolated in each finite element as follows:

$$U_i = \Phi_\alpha U_{\alpha i}, \qquad U_i^* = \Phi_\alpha U_{\alpha i}^*, \tag{15}$$

$$p = \Phi_\alpha p_\alpha, \qquad p^* = \Phi_\alpha p_\alpha^*, \tag{16}$$

where the $\Phi_\alpha$ denote the interpolation functions for velocity and pressure. $U_{\alpha i}$ and $p_\alpha$ are the velocity and pressure at the $\alpha$th node of each finite element. $U_{\alpha i}^*$ and $p_\alpha^*$ are the nodal values of the weighting functions. Standard linear interpolation functions based on the three-node triangular finite element are used.

Substituting equations (15) and (16) in equations (12)–(14), the following finite element equations are derived:

$$\bar{M}_{\alpha\beta}^{n+1} \tilde{U}_{\beta i}^{n+1} = \bar{M}_{\alpha\beta}^n U_{\beta i}^n - \Delta t(S_{\alpha i\beta j}^n U_{\beta j}^n - N_\alpha^n f_i^n - \hat{\Omega}_{\alpha i}^n), \tag{17}$$

$$A_{\alpha i\beta i}^{n+1} p_\beta^{n+1} = -(1/\Delta t) H_{\alpha\beta i}^{n+1} \tilde{U}_{\beta i}^{n+1} + \hat{\Sigma}_\alpha^{n+1}, \tag{18}$$

$$\bar{M}_{\alpha\beta}^{n+1} U_{\beta i}^{n+1} = \bar{M}_{\alpha\beta}^{n+1} \tilde{U}_{\beta i}^{n+1} - \Delta t H_{\alpha\beta i}^{n+1} p_\beta^{n+1}, \tag{19}$$

where

$$M_{\alpha\beta} = \int_V (\Phi_\alpha \Phi_\beta)\mathrm{d}V,$$

$$S_{\alpha i\beta j} = -\upsilon\left(\int_V (\Phi_{\alpha,k}\Phi_{\beta,k}\,\delta_{ij})\mathrm{d}V + \int_V (\Phi_{\alpha,i}\Phi_{\beta,j})\mathrm{d}V\right),$$

$$A_{\alpha i\beta i} = \int_V (\Phi_{\alpha,i}\Phi_{\beta,i})\mathrm{d}V,$$

$$H_{\alpha\beta i} = \int_V (\Phi_\alpha \Phi_{\beta,i})\mathrm{d}V,$$

$$N_\alpha = \int_V (\Phi_\alpha) \mathrm{d}V,$$

$$\hat{\Omega}_{\alpha i} = \int_S [\Phi_\alpha \upsilon (U_{i,j} + U_{j,i}) n_j] \mathrm{d}S = \int_S (\Phi_\alpha \hat{T}_i) \mathrm{d}S,$$

$$\hat{\Sigma}_\alpha = \int_S (\Phi_\alpha p_{,i} n_i) \mathrm{d}S = \int_S (\Phi_\alpha \hat{Q}) \mathrm{d}S.$$

$\bar{M}_{\alpha\beta}$ in equations (17) and (19) is the lumped coefficient derived from $M_{\alpha\beta}$.

The calculation procedure for this method is as follows.

1. Assign $U_i^{n+1(m)} = U_i^n$.
2. Calculate the new position of the nodal point by
$$x_i^{n+1(m)} = x_i^n + \Delta t (U_i^{n+1(m)} + U_i^n)/2.$$
3. Calculate $\tilde{U}_i^{n+1(m+1)}$ by equation (17) using the known $U_i^n$.
4. Solve the Poisson equation (18) for $p^{n+1(m+1)}$ using $\tilde{U}_i^{n+1(m+1)}$.
5. Calculate $U_i^{n+1(m+1)}$ by equation (19), correcting $\tilde{U}_i^{n+1(m+1)}$ by $p^{n+1(m+1)}$.
6. Examine whether $U_i^{n+1(m+1)}$ converges sufficiently or not, and if not replace $U_i^{n+1(m)}$ by $U_i^{n+1(m+1)}$ and recalculate from step 2.
7. Continue to calculate until the preassigned final time.

In this procedure, $(m)$ means $m$th approximation.

## 5. SLOSHING WAVE ON A SLOPED WALL

In order to calculate large-amplitude sloshing waves in containers which have roofs or chamfers, it is necessary to consider the treatment of a sloped or multi-sloped wall boundary (Figure 1). The treatment of this boundary as follows.

1. Judge which sloping wall the boundary nodal point lies on.
2. Calculate the components of the unit normal of the boundary wall surface.
3. Compute the tangential velocity $U_t$ of the boundary nodal point and use this $U_t$ to calculate the new position of the nodal point of calculation procedure step 2 of Section 4.
4. Set $U_n$, the component of velocity normal to the wall, to zero.

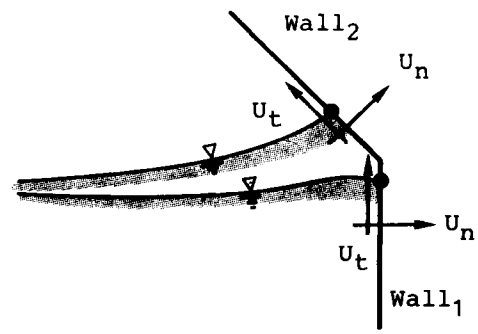


Figure 1. Treatment of a sloped or multi-sloped wall boundary

In this paper an explicit type of numerical integration in time is used. In the scheme, $U_t$ and $U_n$ are corrected at each time step.

As shown in Figure 2, when there are nodal points across a corner of a multi-sloped wall boundary, a 'cave' occurs between the wall and the finite element. In the calculation we assume that the cave is so small that it can be neglected.

## 6. FORCED OSCILLATION OF CONTAINERS

There are two methods of imposing forced oscillation of containers. In the first case the velocity of the wall is imposed as the boundary condition and in the second case the acceleration effect of the container is taken into account as the $f_i$ in equation (1). For example, consider a container subjected to a sinusoidal horizontal oscillation $D = A\sin(\omega t)$ as shown in Figure 3, where $A$ is the amplitude of the displacement and $\omega$ is the angular velocity. In the first case the velocity of the

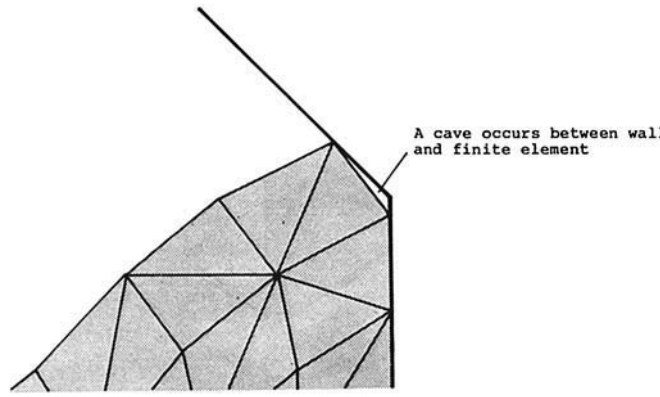


Figure 2. Nodal points across a corner of a multi-sloped wall boundary

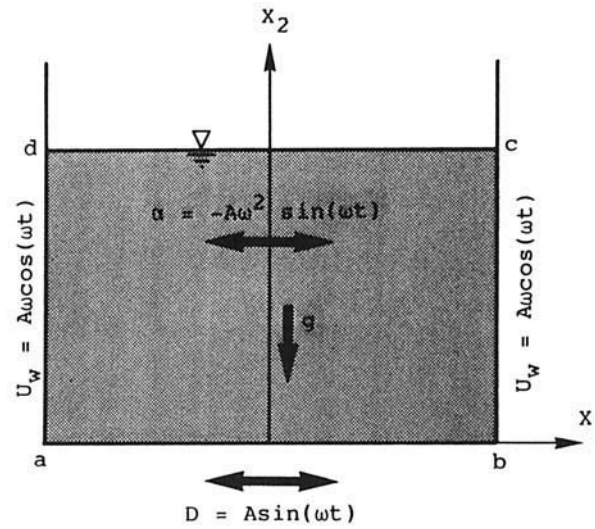


Figure 3. Forced oscillation

wall $U_w = A\omega\cos(\omega t)$ is applied on the boundaries a–d and b–c. In the second case the acceleration $\alpha = -A\omega^2\sin(\omega t)$ is applied as the acceleration $f_2$.

## 7. COMPARISON WITH EXPERIMENTAL RESULTS FOR A RECTANGULAR TANK

To investigate the validity of the present method, a comparison was made with experimental results. A transparent acrylic resin tank 100 cm in width, 120 cm in height and 10 cm in breadth, as shown in Figure 4, was used in the experiment. Water was used as the liquid and the depth was 50 cm. The tank was set on a shaking table which could be oscillated sinusoidally starting from

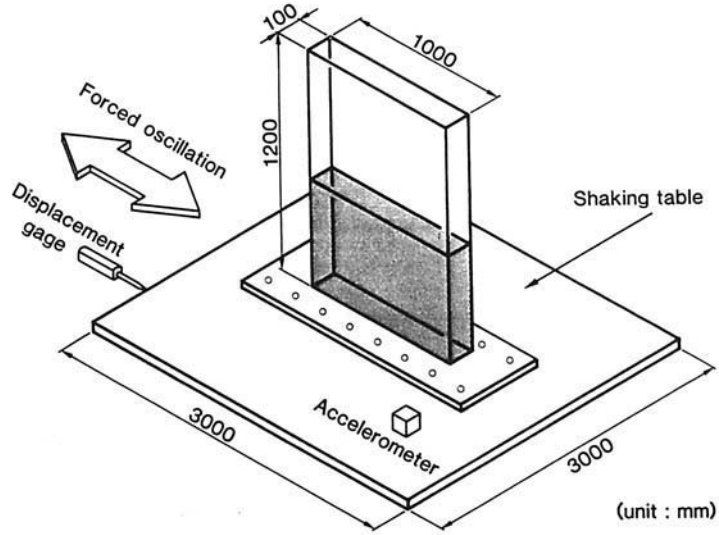


Figure 4. Experimental rectangular model tank set on a shaking table

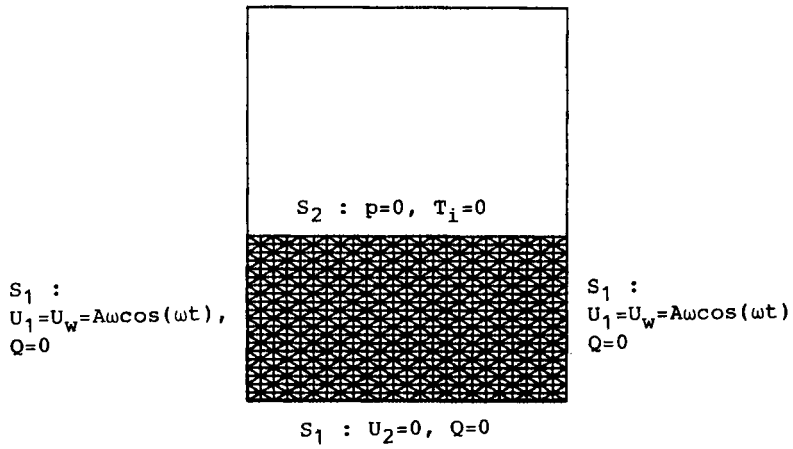


Figure 5. Finite element model

zero velocity. The frequency and amplitude of displacement of the table were measured by a displacement gauge. Sloshing phenomena were recorded by a video camera.

The finite element model is shown in Figure 5. The analytical region is divided into $24 \times 20$ meshes. The density is $1000\,\mathrm{kg\,m^{-3}}$ and the coefficient of kinematic viscosity is $\upsilon = 1{\cdot}0 \times 10^{-6}\,\mathrm{m^2\,s^{-1}}$. The acceleration $f_2$ is $-9{\cdot}8\,\mathrm{m\,s^{-2}}$. The amplitude and period of displacement of the table are 0·93 cm and 1·183 s respectively. The period is nearly equal to the first characteristic period calculated by linear potential theory. The time increment $\Delta t$ is $1{\cdot}0 \times 10^{-4}$ s. The boundary conditions are shown in Figure 5.

Figures 6(a)–6(c) show both the experimental and calculated results. In these figures the left column shows the experimental result while the right three columns show the calculated results of the free surface, the finite element configuration and the pressure distribution. The configurations of the free surface agree well between experimental and calculated results.

## 8. ANALYSIS OF LIQUID IN A CONTAINER

### *8.1. Analysis of liquid in a container inclined instantaneously*

As shown in Figure 7, the container is inclined instantaneously at an angle of 25° and allowed to stand still after the inclination. The dimensions of the container are also shown in the figure. The liquid region is divided into $12 \times 20$ meshes as shown in Figure 8.

In this example the behaviours of two liquids with different viscosities are analysed. The coefficients of kinematic viscosity are $\upsilon = 1{\cdot}0 \times 10^{-3}$ and $5{\cdot}0 \times 10^{-3}\,\mathrm{m^2\,s^{-1}}$ respectively. The density is $1000\,\mathrm{kg\,m^{-3}}$ and the gravitational acceleration $g = 9{\cdot}8\,\mathrm{m\,s^{-2}}$. The time increment $\Delta t$ is $1{\cdot}0 \times 10^{-4}$ s. The boundary conditions are shown in Figure 8.

Figure 9(a)–9(d) show the calculated results. The surface wave is created and climbs up the left wall, is reflected and then travels towards the right wall. For the liquid with the lower viscosity the wave climbing up the left wall is higher and the travelling wave is more predominant.

### *8.2. Analysis of liquid in a container oscillating sinusoidally*

The dimensions of the container are shown in Figure 10. The liquid region is divided into $12 \times 20$ meshes. Figure 11 shows the finite element model. The density is $1000\,\mathrm{kg\,m^{-3}}$ and the coefficient of kinematic viscosity is $\upsilon = 1{\cdot}0 \times 10^{-3}\,\mathrm{m^2\,s^{-1}}$. The acceleration $f_2$ is $-9{\cdot}8\,\mathrm{m\,s^{-2}}$. First the container is at rest and is then moved sinusoidally. The amplitude and period of displacement are 12·5 cm and 1·75 s respectively. The time increment $\Delta t$ in this calculation is $1{\cdot}0 \times 10^{-4}$ s. The boundary conditions are shown in Figure 11.

The calculated results for the finite element configuration and the pressure distribution are shown in Figures 12(a)–12(h). The sloshing wave is seen to grow with time. At $t = 2{\cdot}76$ s the wave covers almost all of the left upper chamfer and the configuration of the free surface is a double-valued function of $x_1$. As the sloshing wave grows, the pressure distribution changes from a static pressure distribution. For example, at $t = 1{\cdot}80$, as shown in Figure 12(f), the sloshing wave climbs up the right wall and the pressure contour lines become sparse in the right region and dense in the left region. At $t = 2{\cdot}52$, as shown in Figure 12(h), the sloshing wave passes the corner of the container and a high pressure occurs near the corner.

At $t = 2{\cdot}76$, as shown in Figure 12(h), the mesh configuration is distorted and the calculation cannot proceed any further. To overcome this problem and to obtain further calculation steps, finite element rezoning of the multi-sloped wall boundary is needed.

The calculations were carried out using a FACOM VP-50 computer system. The CPU times for the calculation of Examples 8.1 and 8.2 were 25 and 40 min respectively.

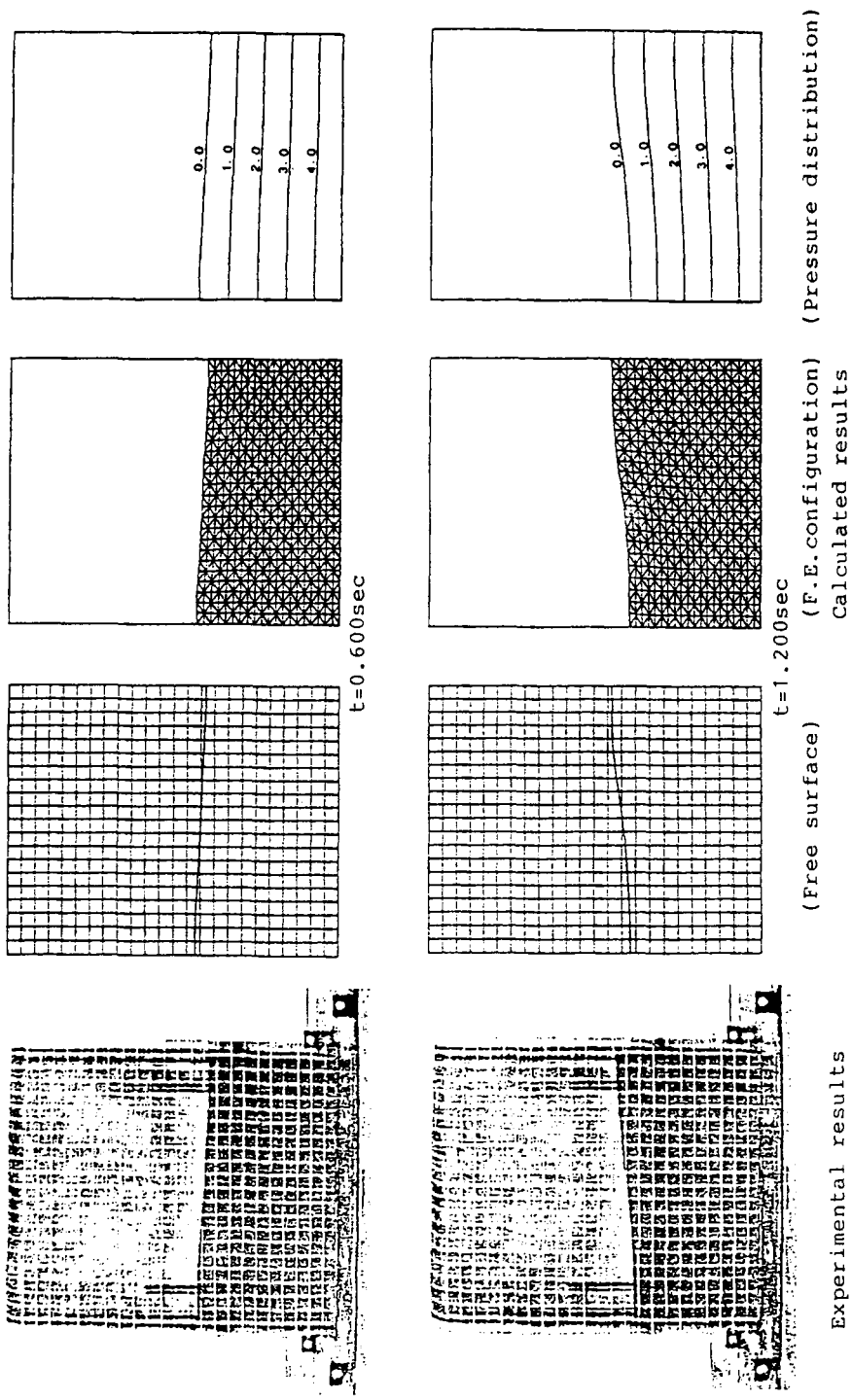


Figure 6(a). Experimental and calculated results

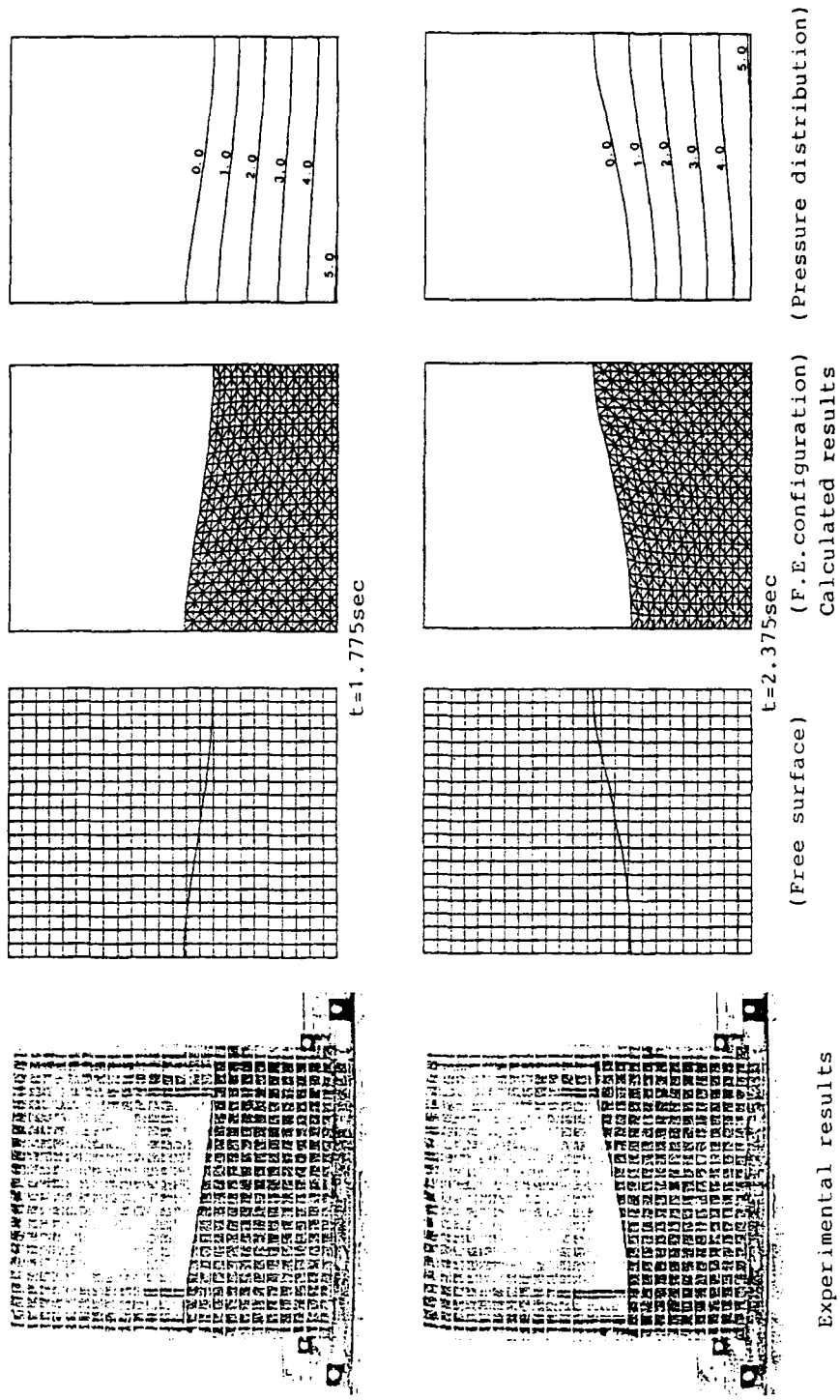


Figure 6(b). Experimental and calculated results

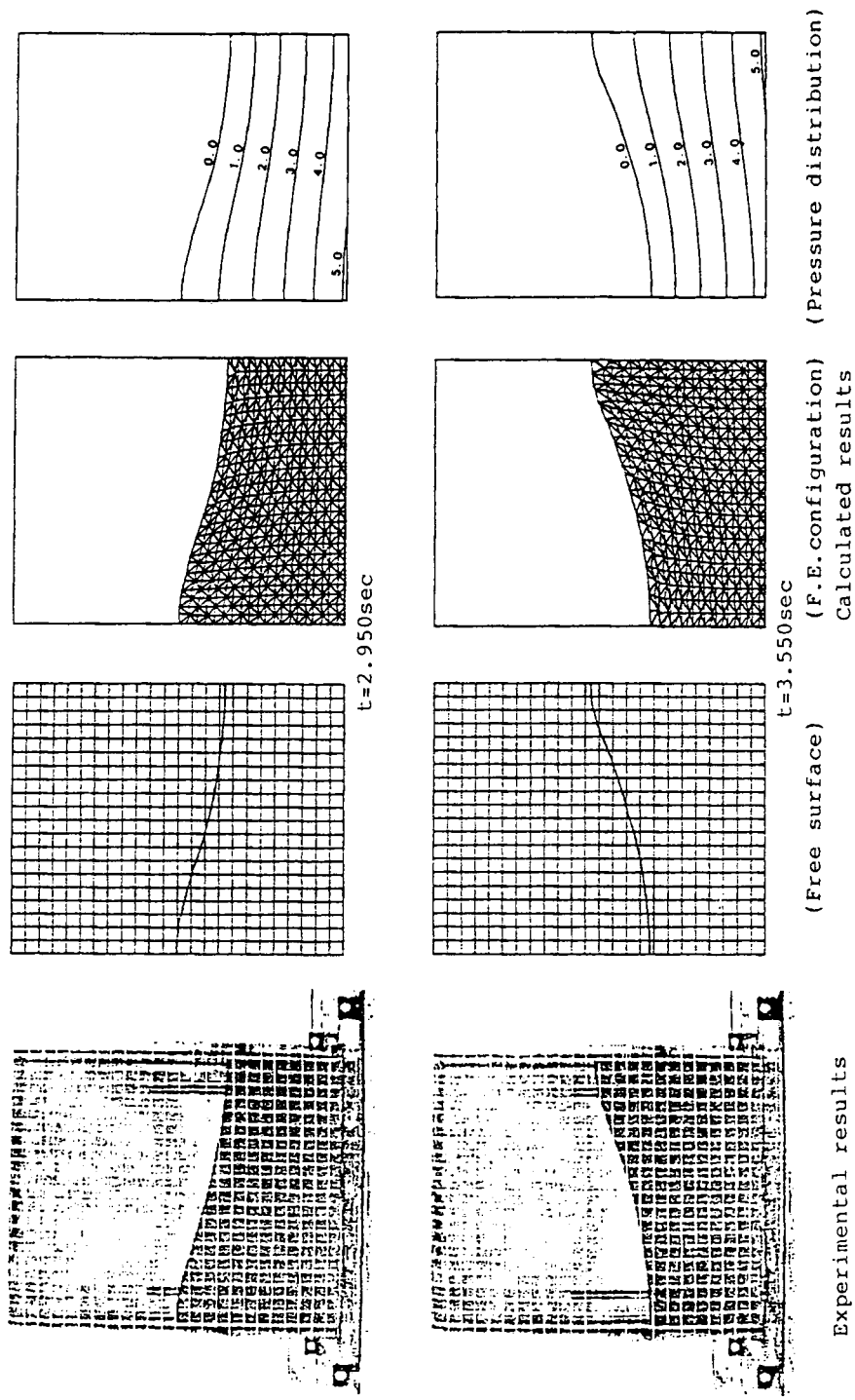


Figure 6(c). Experimental and calculated results

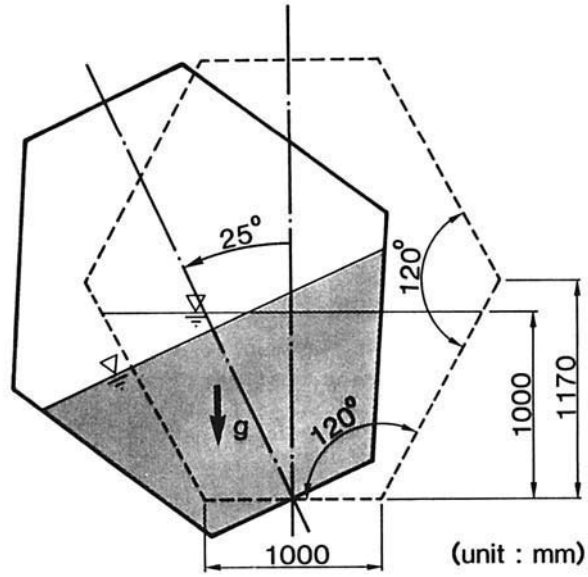


Figure 7. Container of Example 8.1

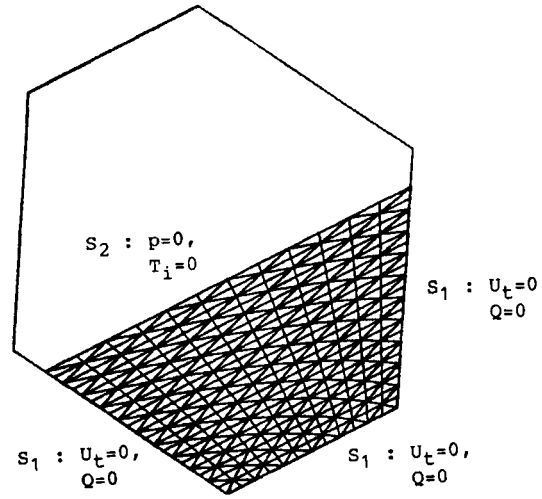


Figure 8. Finite element model

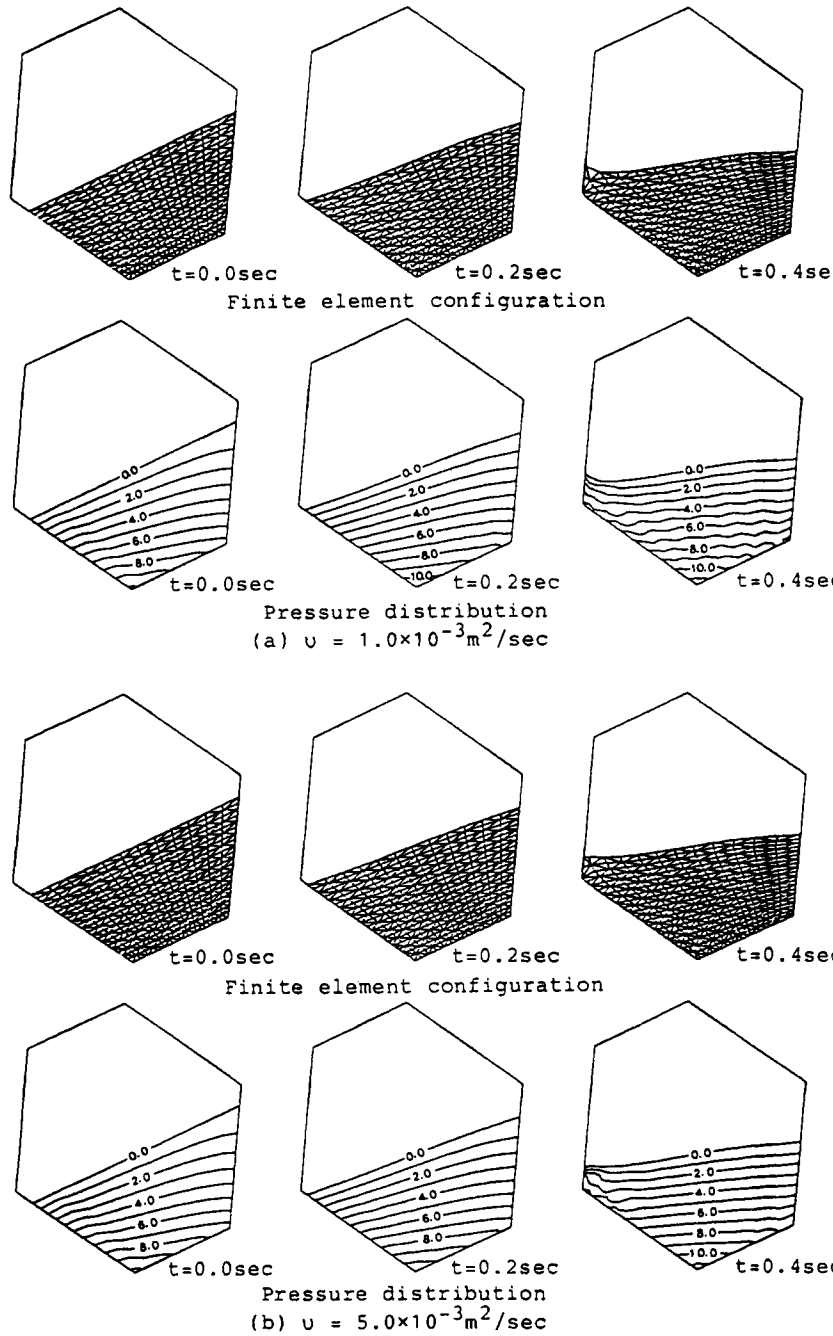


Figure 9(a). Calculated results of Example 8.1

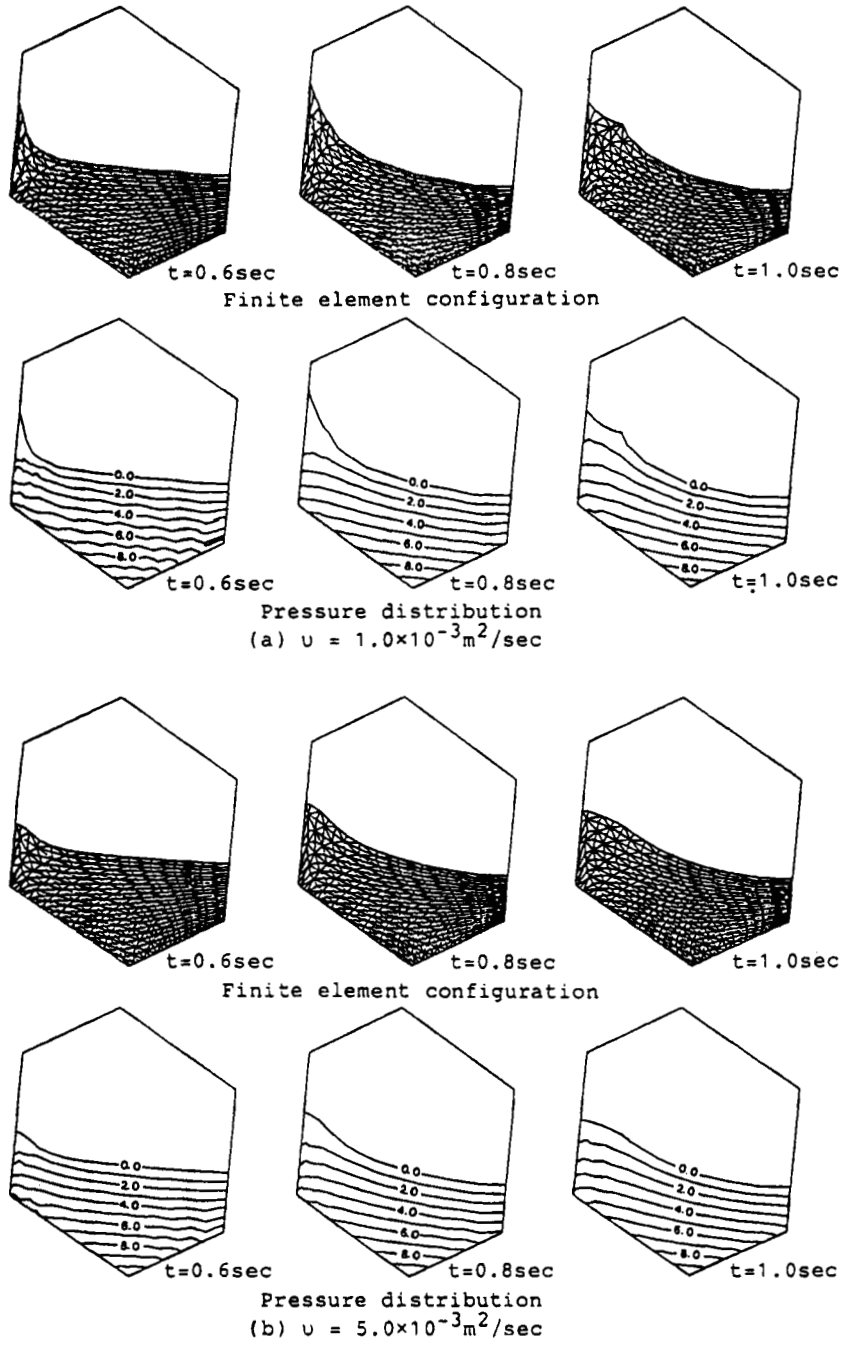


Figure 9(b). Calculated results of Example 8.1

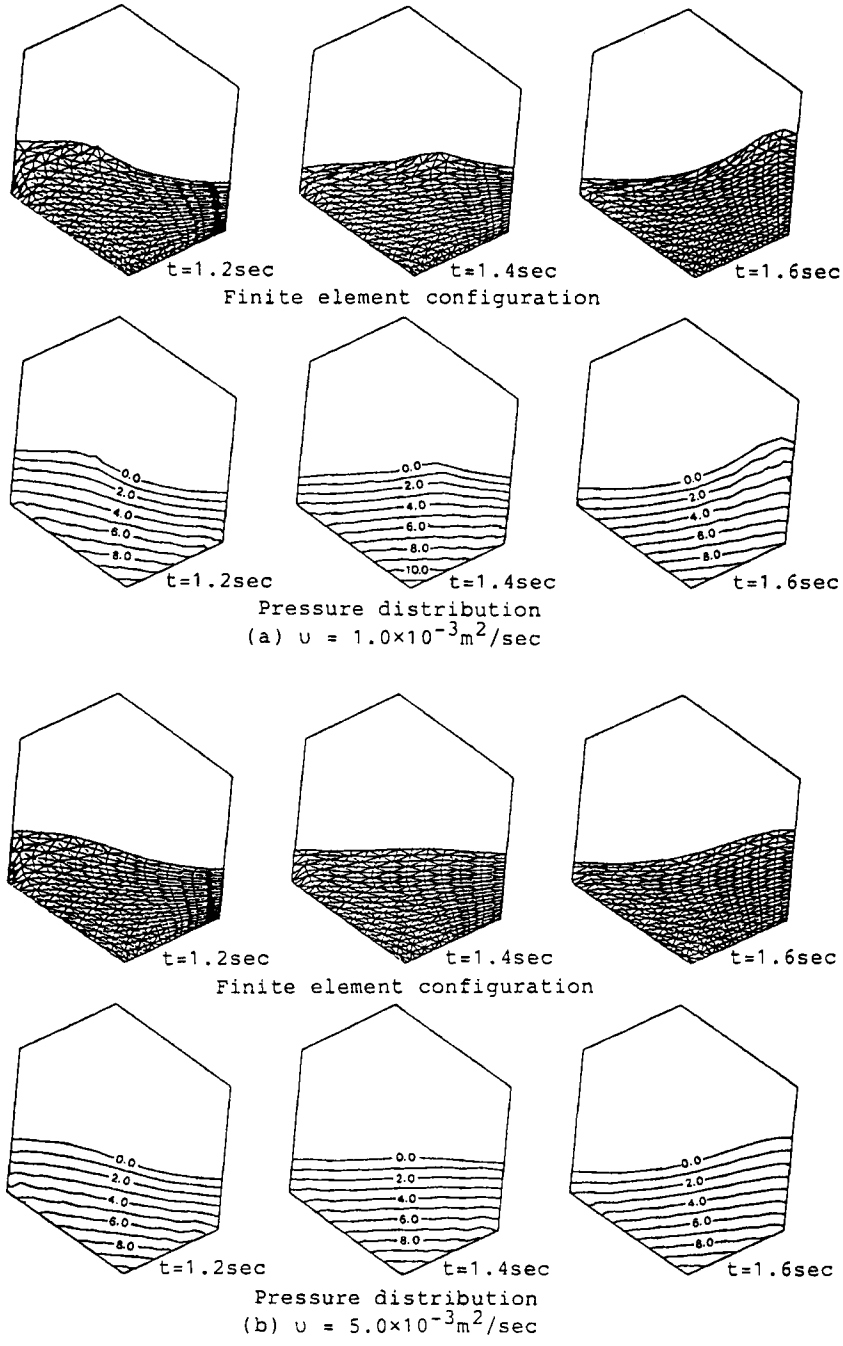


Figure 9(c). Calculated results of Example 8.1

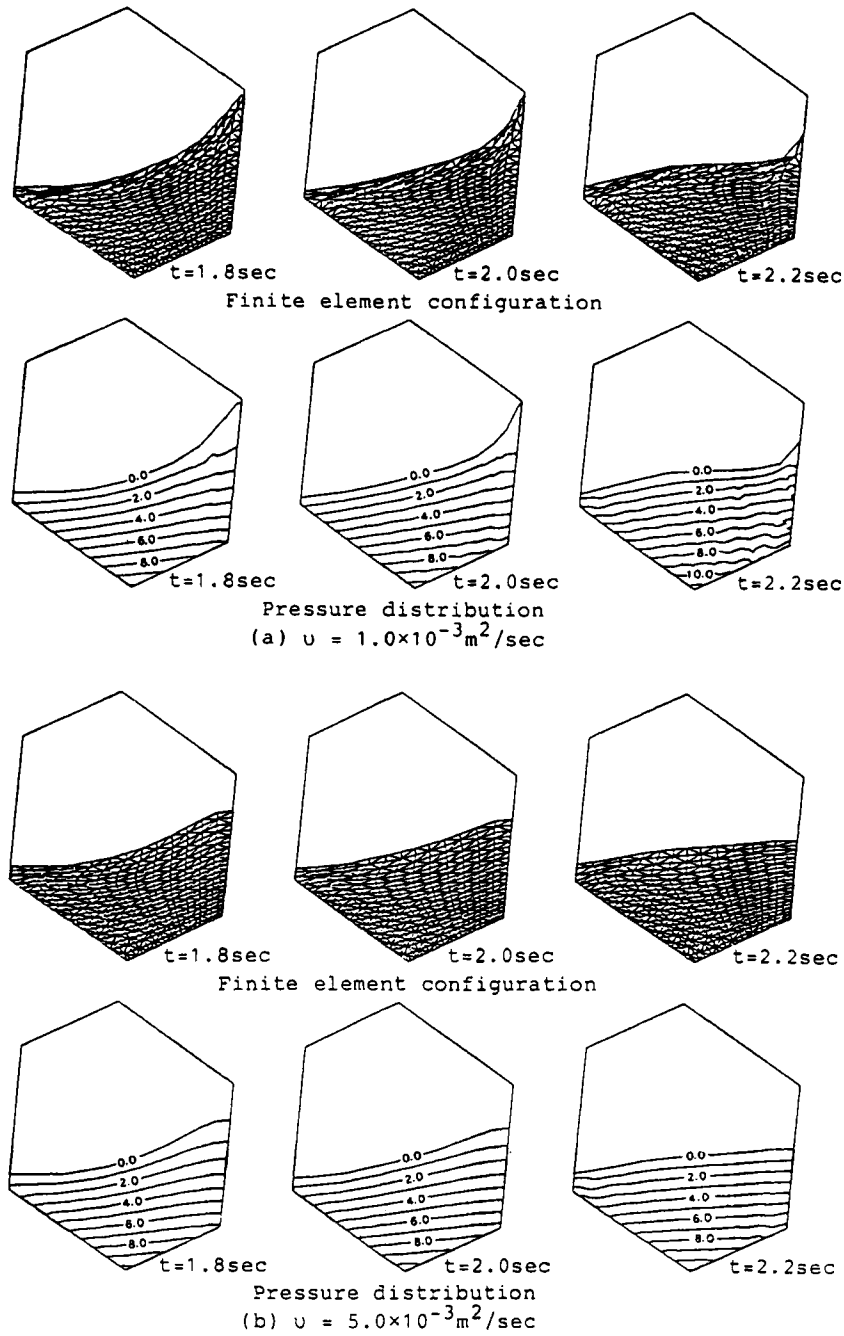


Figure 9(d). Calculated results of Example 8.1

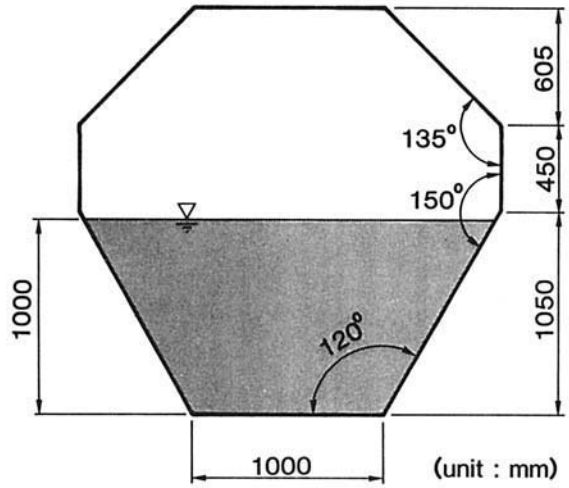


Figure 10. Container of Example 8.2

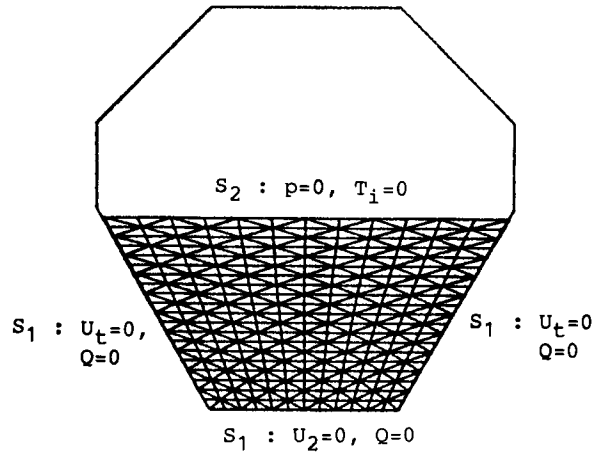


Figure 11. Finite element model

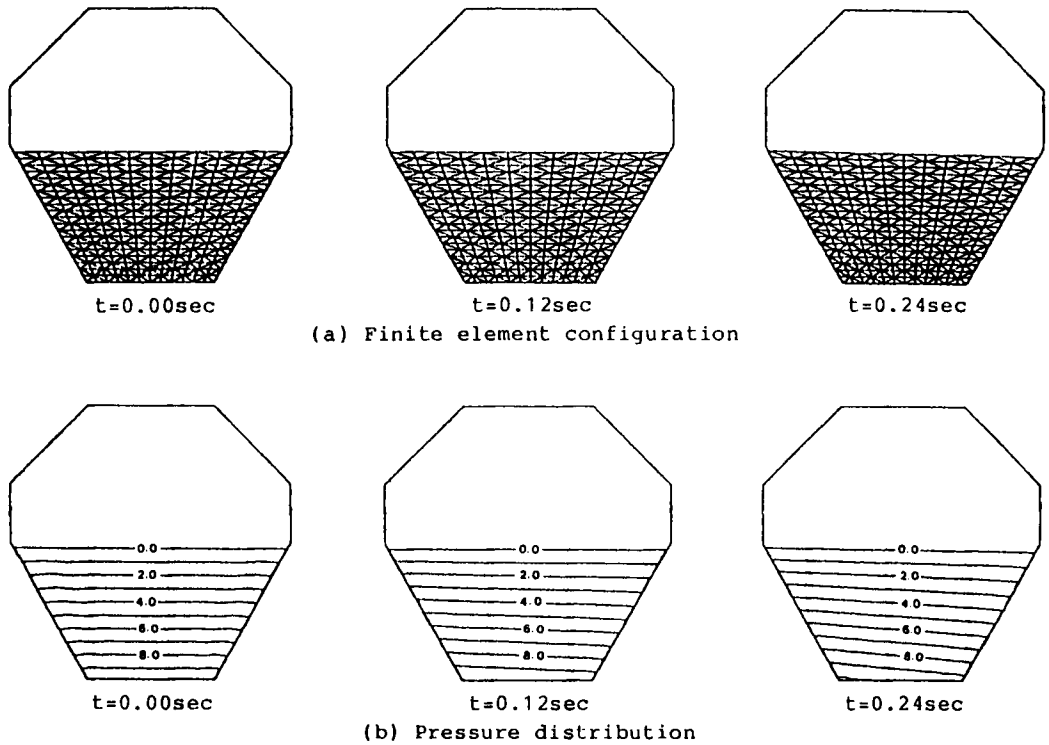


Figure 12(a). Calculated results of Example 8.2

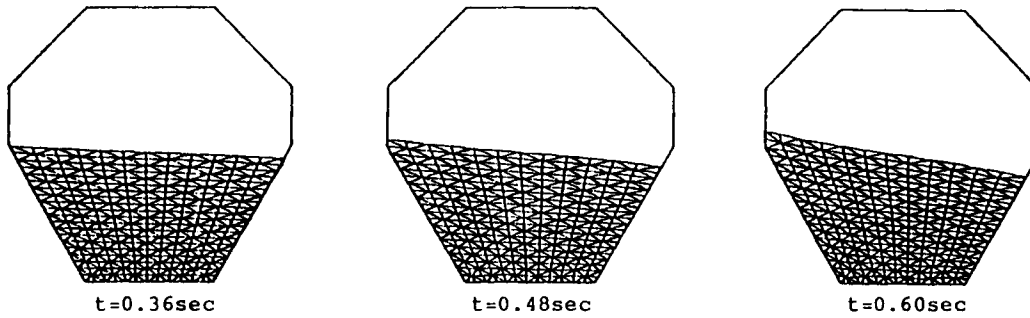


(a) Finite element configuration

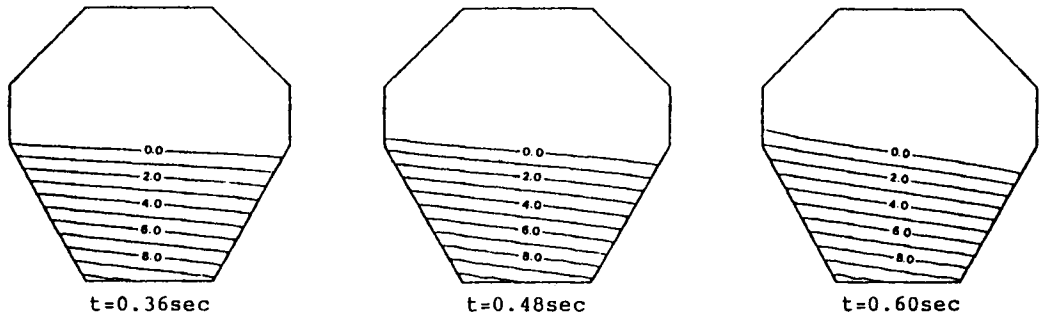


(b) Pressure distribution

Figure 12(b). Calculated results of Example 8.2

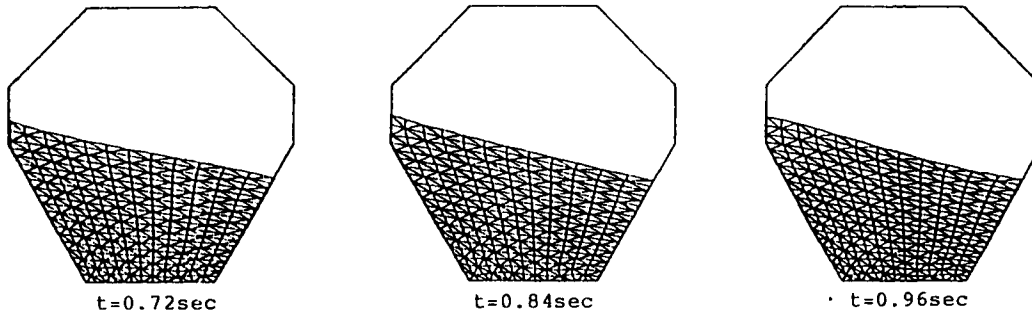


(a) Finite element configuration

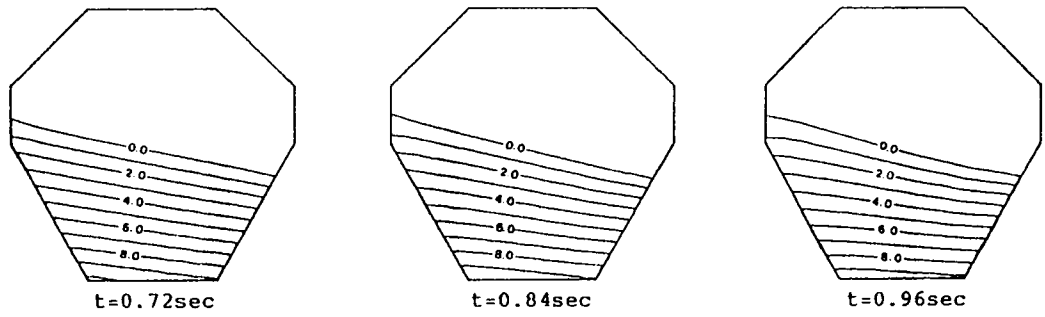


(b) Pressure distribution

Figure 12(c). Calculated results of Example 8.2

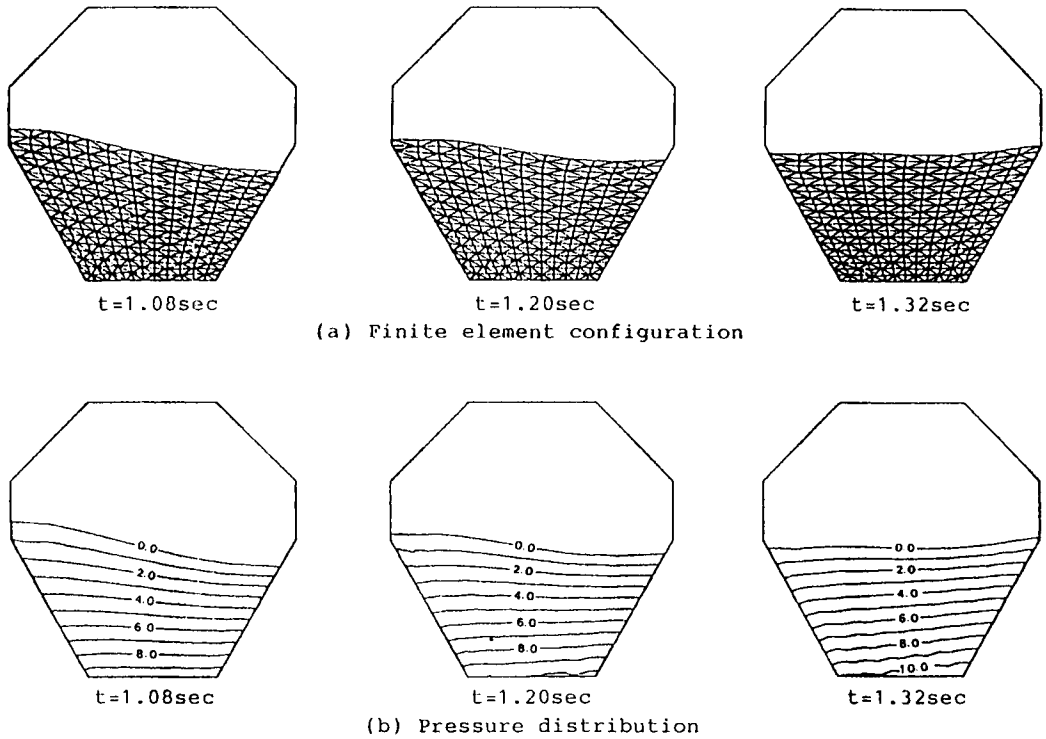


Figure 12(d). Calculated results of Example 8.2

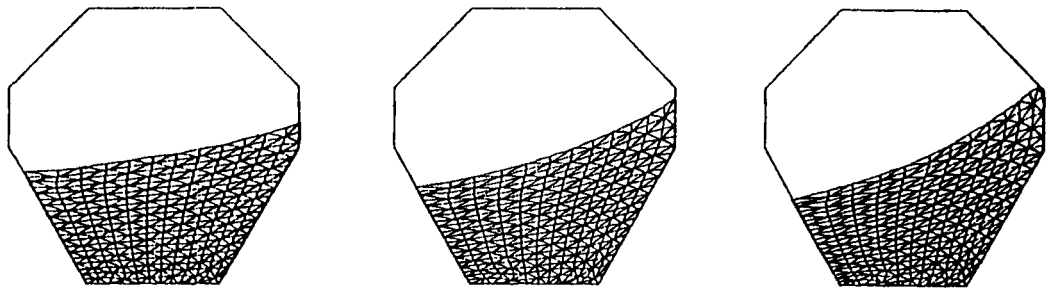


(a) Finite element configuration

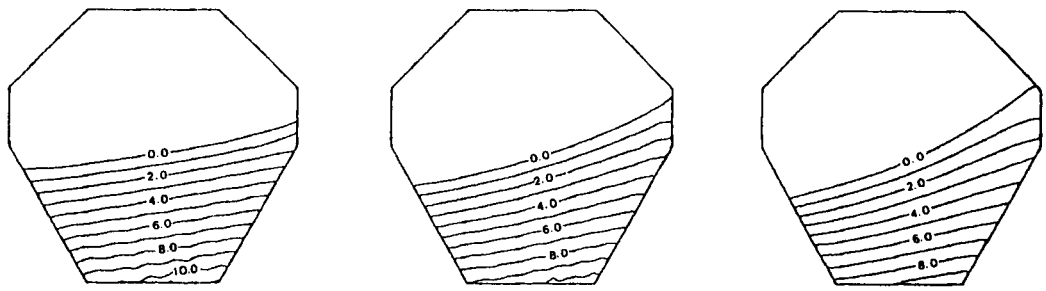


(b) Pressure distribution

Figure 12(e). Calculated results of Example 8.2

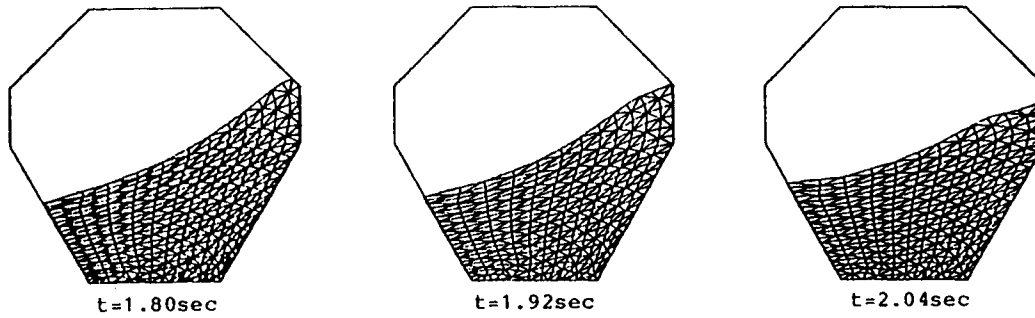


(a) Finite element configuration

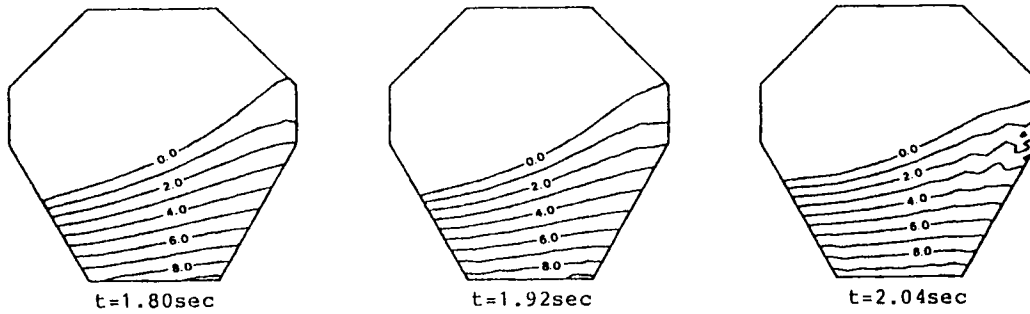


(b) Pressure distribution

Figure 12(f). Calculated results of Example 8.2

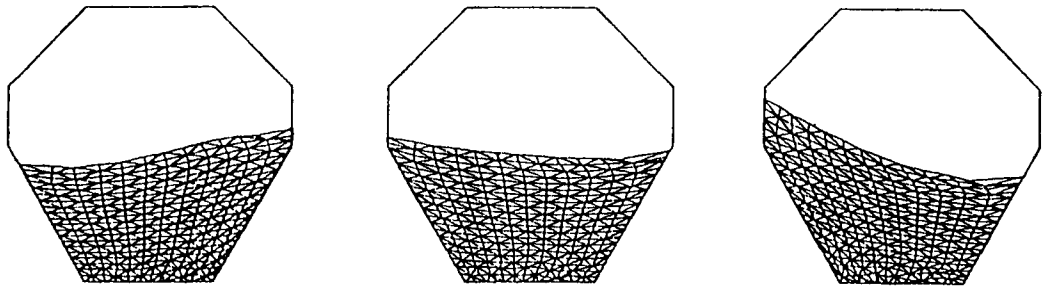


(a) Finite element configuration

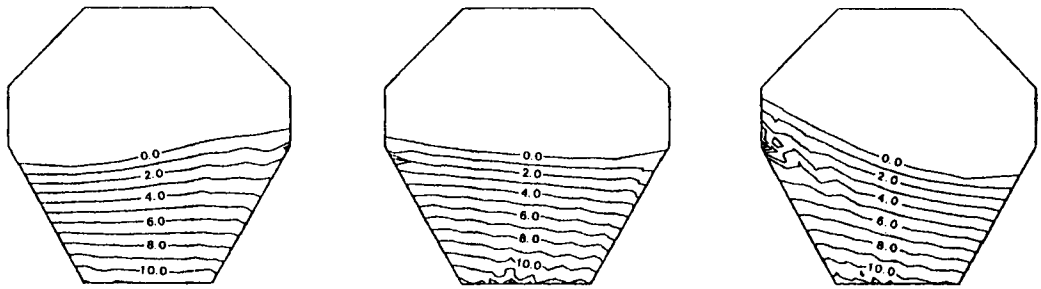


(b) Pressure distribution

Figure 12(g). Calculated results of Example 8.2

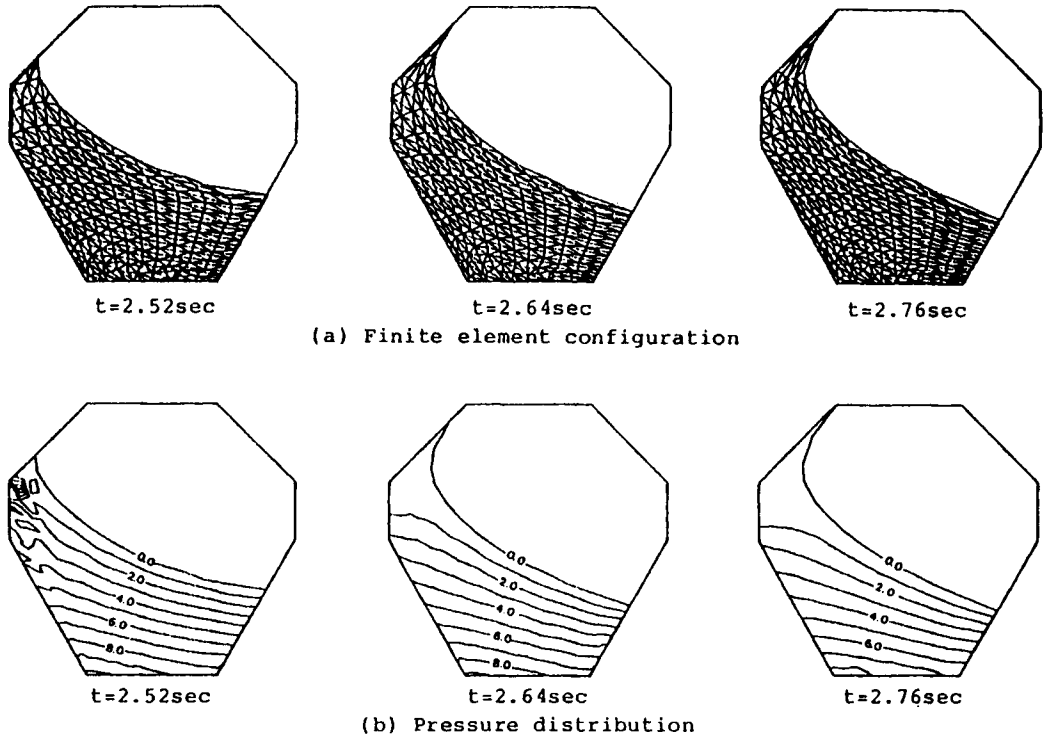


Figure 12(h). Calculated results of Example 8.2

## 9. CONCLUSIONS

Using the Lagrangian finite element method, large-amplitude sloshing waves in a container of complicated shape with roofs or chamfers can be analysed. By comparison with experimental results, this method is shown to be sufficiently accurate to follow the free surface position and to obtain the velocity and pressure distributions. Furthermore, two examples are presented to validate the ability to calculate large-amplitude sloshing waves. In the last example the wave is so high that the configuration of the free surface is a double-valued function of the horizontal co-ordinate.

ACKNOWLEDGEMENTS

The authors wish to thank Dr. B. Ramaswamy, Dr. T. Nakayama and Dr. H. Nagaoka for helpful discussions. A part of this research was supported by Grant in Aids in Science and Engineering, Ministry of Education, Government of Japan.

REFERENCES

1. G. W. Housner, 'Dynamic pressures on accelerated fluid containers', *Bull. Seismol. Soc. Am.*, **47**, 15–35 (1957).
2. S. Silverman and H. N. Abramson, 'Lateral sloshing in moving containers', *NASA SP-106*, 1966, pp. 13–78.
3. K. Sogabe and A. Shibata, 'Response analysis on sloshing of liquid in a cylindrical storage. I—Basic equation and response to sinusoidal input', *Seisan Kenkyu*, **26**, 119–122 (1974).
4. T. Okamoto, Y. Yamada and S. Noda, 'Estimation of sloshing wave height in vicinity of source region', *Proc. Ninth World Conf. on Earthquake Engineering*, **4**, 607–612 (1988).

5. H. N. Abramson, W. H. Chu and F. T. Dodge, 'Nonlinear effects in lateral sloshing', *NASA SP-106*, 1966, pp. 79–103.
6. F. H. Harlow and J. E. Welch, 'Numerical calculation of time-dependent viscous incompressible flow of fluid with free surface', *Phys. Fluids*, **8**, 2182–2189 (1965).
7. F. H. Harlow and J. E. Welch, 'Numerical study of large-amplitude free-surface motions', *Phys. Fluids*, **9**, 842–851 (1966).
8. T. Nakayama and K. Washizu, 'Nonlinear analysis of liquid motion in a container subjected to forced pitching oscillation', *Int. j. numer. methods eng.*, **15**, 1207–1220 (1980).
9. K. Washizu, 'Some applications of finite element techniques to nonlinear free surface fluid flow problems', *Finite Element Flow Analysis, Proc. Fourth Int. Symp. on Finite Element Methods in Flow Problems*, 1982, pp. 3–15.
10. T. Hino, H. Miyata and H. Kajitani, 'A numerical solution method for nonlinear shallow water waves (first report)', *J. Soc. Naval Architects Jpn.*, **153**, 37–48 (1983).
11. T. Hino, H. Miyata, H. Kajitani and M. Kanai, 'A numerical solution method for nonlinear shallow water waves (second report)', *J. Soc. Naval Architects Jpn.*, **154**, 29–39 (1984).
12. B. Ramaswamy, M. Kawahara and T. Nakayama, 'Lagrangian finite element method for the analysis of two-dimensional sloshing problems', *Int. j. numer. methods fluids*, **6**, 659–670 (1986).
13. B. Ramaswamy and M. Kawahara, 'Lagrangian finite element analysis applied to viscous free surface fluid flow', *Int. j. numer. methods fluids*, **7**, 953–984 (1987).
14. B. Ramaswamy and M. Kawahara, 'Arbitrary Lagrangian–Eulerian finite element method for unsteady, convective, incompressible viscous free surface fluid flow', *Int. j. numer. methods fluids*, **7**, 1053–1075 (1987).
15. M. Kawahara and A. Anjyu, 'Lagrangian finite element method for solitary wave propagation', *Comput. Mech.*, **3**, 299–307 (1988).
16. T. Okamoto, M. Kawahara and N. Nagaoka, 'Sloshing analysis by Lagrangian finite element method', *Computational Methods in Flow Analysis, Proc. Int. Conf. on Computation Method in Flow Analysis, Vol. 2*, Okayama, 1988, pp. 1049–1056.
17. C. W. Hirt and J. P. Shannon, 'Free-surface stress conditions for incompressible-flow calculations', *J. Comput. Phys.*, **2**, 403–411 (1968).
18. B. D. Nichols and C. W. Hirt, 'Improved free surface boundary conditions for numerical incompressible-flow calculations', *J. Comput. Phys.*, **8**, 434–448 (1971).
19. J. A. Viecelli, 'A method for including arbitrary external boundaries in the MAC incompressible fluid computing technique', *J. Comput. Phys.*, **4**, 543–551 (1969).
20. J. A. Viecelli, 'A computing method for incompressible flows bounded by moving walls', *J. Comput. Phys.*, **8**, 119–143 (1971).
21. T. Hino, H. Miyata and H. Kajitani, 'Numerical simulation of nonlinear behavior of three-dimensional ocean waves interacting with obstacles', *J. Soc. Naval Architects Jpn.*, **157**, 141–154 (1985).
22. J. F. Dalzell, 'Simulation and experimental techniques Part I. Simulation of liquid sloshing', *NASA SP-106*, 1966, pp. 145–169.
23. G. W. Brooks, 'Simulation and experimental techniques Part II. Experimental techniques and apparatus', *NASA SP-106*, 1966, pp. 170–197.